FORECASTING INFLUENZA HOSPITALIZATIONS USING A BAYESIAN HIERARCHICAL NONLINEAR MODEL WITH DISCREPANCY

Spencer Wadsworth

University of Connecticut Storrs, Connecticut iac25002@uconn.edu Jarad Niemi

Iowa State University
Ames, Iowa
niemi@iastate.edu

ABSTRACT

The annual influenza outbreak leads to significant public health and economic burdens making it desirable to have prompt and accurate probabilistic forecasts of the disease spread. The United States Centers for Disease Control and Prevention hosts annually a national flu forecasting competition which has led to the development of a variety of flu forecast modeling methods. For the first several years of the competition, the target to be forecast was weekly percentage of patients with an influenzalike illness (ILI), but in 2021 the target was changed to weekly hospitalization counts. Reliable state and national hospitalization data has only been available since 2021, but for ILI the data has been available since 2010 and has been successfully forecast for several seasons. In this manuscript, we introduce a two component Bayesian modeling framework for forecasting weekly hospitalizations utilizing both hospitalization data and ILI data. The first component is for modeling ILI data using a nonlinear Bayesian hierarchical model. This component includes modeling discrepancy between a nonlinear functional model and the observed ILI which requires thoughtful decisions for modeling constraints and selecting prior parameter distributions. The second component is for modeling hospitalizations as a function of ILI. For hospitalization forecasts, ILI is first forecasted and then hospitalizations forecasts are produced using ILI forecasts as a linear or quadratic predictor. The combination of the models is done in a manner similar to using the Bayesian cut. In a simulation study, two ILI forecast models, including one similar to the winning model for two seasons of the CDC forecast competition from Osthus et al. and a nonlinear Bayesian hierarchical model from Ulloa are compared with other standard forecasts models. The usefulness of including a systematic model discrepancy term in the ILI model is specifically addressed and proves to greatly improve forecasts. In a real data analysis, forecasts of state and national hospitalizations for the 2023-24 flu season are made and compared with forecasts from 20 other competing models. The forecasts from the proposed methodology outperformed all but one of 20 competing models.

 $\textbf{\textit{Keywords}}$ Disease outbreak forecasting \cdot Bayesian hierarchical modeling \cdot Probabilistic forecasting \cdot Model discrepancy

1 Introduction

Every year the seasonal influenza outbreak burdens the public health system by infecting millions, causing an influx of primary care visits and hospitalizations and leading to between 290,000 and 650,000 deaths worldwide [WHO, 2024]. Molinari et al., 2007] estimated the United States' annual economic burden from medical costs, loss of income, and deaths to be over \$87 billion. Accurate forecasting of infectious diseases can inform public decision making and ease the burden of an outbreak [Turtle et al., 2021, Lutz et al., 2019]. There is a growing consensus that disease forecasts should be probabilistic in nature [Gneiting and Katzfuss, 2014, Bracher et al., 2021], and it has been shown that reporting forecast uncertainty along with predictions may lead to better decision making [Ramos et al., 2013, Joslyn and LeClerc, 2012, Winkler, 1971].

To better inform public decision making regarding the flu epidemic, in 2013 the United States Centers for Disease Control and Prevention (CDC) organized a national flu forecasting competition, also known as FluSight [Biggerstaff et al., 2016, Mathis et al., 2024, CDC, 2024b]. The competition lasted from the fall of 2013 through spring of 2014, and originally over a dozen teams of researchers from academic and industry backgrounds participated in FluSight by contributing their own forecast models. Besides the 2020-21 season, FluSight has been operated annually and researchers outside the CDC have been invited to participate. From hereon, we denote a flu season by the year in which the outbreak began, i.e. the 2020 season season outbreak began in 2020 and lasted until spring 2021. Initially the target data for forecasts was influenza-like illness (ILI) data. ILI is the proportion of patients who meet a healthcare provider and who display flu like symptoms, and ILI data has been available at the state and national level since the 2010 flu season [CDC, 2024c,a]. The collaborative ILI forecasting effort has led to a number of modeling developments in flu forecasting [McAndrew and Reich, 2021, Osthus and Moran, 2021, Osthus et al., 2019, Ulloa, 2019, see references therein for more examples], and in their introduction, Osthus et al. [Osthus et al., 2019] categorized the most commonly used flu forecasting models into four classes including mechanistic models based on differential equation compartmental models, agent based models based on population simulation, machine learning/regression models including data driven machine learning and statistical models, and data assimilation models which are constructed by assimilating mechanistic models into a probabilistic framework. An additional forecast modeling class used in FluSight involves the combination of several forecasts into a single ensemble forecast, which has been shown to perform well relative to individual models [McAndrew and Reich, 2021, Ray et al., 2020, Yamana et al., 2016].

The administration of FluSight saw few changes during the first seven seasons between 2013 and 2019, but the onset of the COVID-19 pandemic and subsequent developments for COVID-19 forecasting led to major modifications. As a result of the COVID-19 pandemic which began during the 2019 flu season, the typical flu outbreak behavior was altered between the 2019 and 2022 seasons [Mathis et al., 2024]. The COVID-19 pandemic led to the creation of the Health and Human Services (HHS) Patient Impact and Hospital Capacity Data System [HealthData.gov, 2024] which contains COVID-19 and flu hospitalization data, and the COVID-19 Forecast Hub was founded. The COVID-19 Forecast Hub was based on FluSight but with certain major adjustments including how the forecast uncertainty is represented and the addition of the weekly publication of a multi-model ensemble forecast as the official forecast of the CDC [Bracher et al., 2021, Cramer et al., 2022]. Using estimated quantiles for representing forecast uncertainty and creating a multi-model ensemble are both aspects of the COVID-19 Forecast Hub which were adopted by FluSight. Additionally the target of the flu forecasts changed from being ILI data to being HHS hospitalization data, which reports the number of hospitalizations due to a laboratory confirmed flu infection [Mathis et al., 2024, HealthData.gov, 2024]. This in part was as a result of having COVID-19 cases in the population making ILI data, already only a proxy for flu behavior, more difficult to interpret.

The contribution of this manuscript is to introduce a two component Bayesian modeling framework for modeling HHS hospitalization forecasts where hospitalization data and years of ILI data are used to inform forecast models. The first modeling component is a hierarchical model of ILI data. The second is a model of hospitalization data with ILI as a predictive covariate. Herein we use Bayesian ILI models similar to those in Osthus et al. [Osthus et al., 2019] and Ulloa [Ulloa, 2019] for ILI forecasting. The model of Osthus et al. [Osthus et al., 2019] is a combined data assimilation and statistical regression model which involves a compartmental model in a probabilistic framework. Their model also includes an additional component for capturing a systematic discrepancy between the deterministic part of the model and the actual data, an idea which was first introduced by Kennedy and O'Hagan [Kennedy and O'Hagan, 2001]. The model in Ulloa [Ulloa, 2019] is a Bayesian hierarchical regression model with an underlying function intended to capture the trajectory of the seasonal ILI data. Herein, we provide a framework under which discrepancy modeling may be used along with a general function modeling ILI data. Modeling discrepancy introduced challenges which required thoughtful selection of model constraints and prior distributions to be used effectively.

In line with the newer FluSight standard of forecasting hospitalizations, we model hospitalizations as a linear function of ILI. The flu hospitalization forecasts are a linear mapping of ILI forecasts allowing for ILI data from many seasons to be exploited and assist in forecasting hospitalizations. To produce hospitalization forecasts, a scheme similar to the Bayesian cut is used where forecasts from the posterior predictive distribution of an ILI model are plugged into the hospitalization model to produce a posterior predictive hospitalization forecast distribution. We show that this scheme produces accurate and reasonably well calibrated probabilistic forecasts. The forecasts produced in this manuscript are compared with out of the box forecast models in a simulation study, and in a real data analysis the forecasts are compared with 20 other forecasts from the 2023 FluSight forecast competition. The proposed models outperform both the out of the box methods, and they outperform all but one of the FluSight models.

In section 2 we review the ILI and hospitalization data provided by the CDC and targeted by FluSight. In section 3 the modeling framework contributed by this manuscript is given. In the same section, functions similar to those used by Osthus et al. [Osthus et al., 2019] and Ulloa [Ulloa, 2019] are defined. These functions are the susceptible-infectious-recovered (SIR) compartmental model and the asymmetric Gaussian (ASG) function respectively. Model fitting and

implementation are described at the end of the section. Section 4 includes a simulation study where four ILI forecast models and their use in forecasting hospitalizations are compared. Commonly used proper scoring rules [Gneiting and Raftery, 2007] are used for comparing the forecasts. Forecasting of the 2023 flu outbreak along with assessment and comparison of 20 FluSight models is performed in section 5. Finally, the manuscript is concluded in section 6 with general observations and some discussion.

2 Flu outbreak data

In this section we introduce, define, and visually evaluate ILI and hospitalization data. ILI and hospitalization data have been the object of forecasting for FluSight with ILI being the target for the first seven seasons, 2013 to 2019, and hospitalizations being the target since the 2022 season. Both of these data were collected at the state, territorial, and national levels and were reported at least weekly. Overall the data is reported for 53 locations including the 50 US states, the District of Columbia (DC), Puerto Rico (PR), and the US national level. We will refer to forecast targets throughout this manuscript. A target is the specific horizon, 1, 2, 3, or 4-weeks ahead, for a specific location and week during the season.

2.1 Influenza-like illness data

The US Outpatient Influenza-like Illness Surveillance Network collects information on respiratory illness from outpatient visits to health care providers. Each week, over 3,400 outpatient health care providers in all 50 US states, PR, DC, and the US Virgin Islands report the total number of outpatient visits along with the number of ILI cases. An ILI case is defined as a "fever (temperature of 100° F[37.8°C] or greater) and a cough and/or a sore throat." Prior to the 2021 season, the definition included "without a known cause other than influenza" [CDC, 2024c]. Because other illnesses such as COVID-19, RSV, and the common cold may induce similar respiratory symptoms, ILI may include patients infected with some disease other than influenza. To know whether or not a sick patient is infected with influenza requires a laboratory test.

In 2013, when FluSight began, the ILI data was the object of the forecasts. The data was released publicly at HHS region levels, and forecast teams were asked to provide forecasts of several ILI targets on the regional levels including season onset, 1-4 week ahead ILI levels, and the week of peak ILI activity [Biggerstaff et al., 2016, McGowan et al., 2019]. Currently, the ILI data is collected by the CDC and published on an online portal for viewing at the national, HHS region, census, and state levels [CDC, 2024a]. To obtain ILI data, we used the R package cdcfluview which provides functions for downloading the data [Rudis, 2021]. Weekly ILI data from the national, HHS region, and census levels are available from the 1997 flu season up to the current season. At the state level, data is available from the 2010 flu season to the current season.

The top of figure 1 shows the ILI data at the national level for flu seasons 2010 to 2023. For most seasons there are 52 weeks listed, but for the 2010, 2015, and 2021 seasons there are 53 weeks because those seasons had 53 Sundays. To better align with the flu behavior, week 1 is set as the first week of August and week 52 or 53 is the last week in July of the following year. For example, week 1 of the 2013 season corresponds to the first week of August 2013, and week 52 of the same season corresponds to the last week of July 2014. This convention is used for the remainder of this manuscript.

Notable from the plots in the top of figure 1 is the regular trajectory of the ILI. With the exception of season 2020, the ILI begins low at week 1 and increases as the fall and winter progress until the ILI reaches a peak. As spring progresses to summer, the ILI decreases to low values. As Osthus et al. [Osthus et al., 2019] point out, there is nearly always either a global or local peak at week 22 which typically corresponds to the week between Christmas and New Year's day. Whether local or global, the ILI holiday peak is generally expected and thought to be due to widespread holiday travel, school closure, or other unique social behavior [Ewing et al., 2017, Garza et al., 2013]. The only seasons when there was not a peak at week 22 were 2022, when the season peak occurred particularly early, and 2020 which was greatly influenced by the COVID-19 pandemic.

2.2 Hospitalization Data

Weekly hospital admission data, which was used as the object of FluSight forecasting for the 2022 and 2023 seasons, is based on the CDC's National Healthcare Safety Network (NHSN) dataset entitled *HealthData.gov COVID-19 Reported Patient Impact and Hospital Capacity by State Timeseries*. In February 2022 it became mandatory for all hospitals to report the number of COVID-19 and influenza hospitalizations, and since then reporting of hospitalizations has become widespread. These data were updated every Wednesday and Friday according to NHSN guidelines [HealthData.gov,

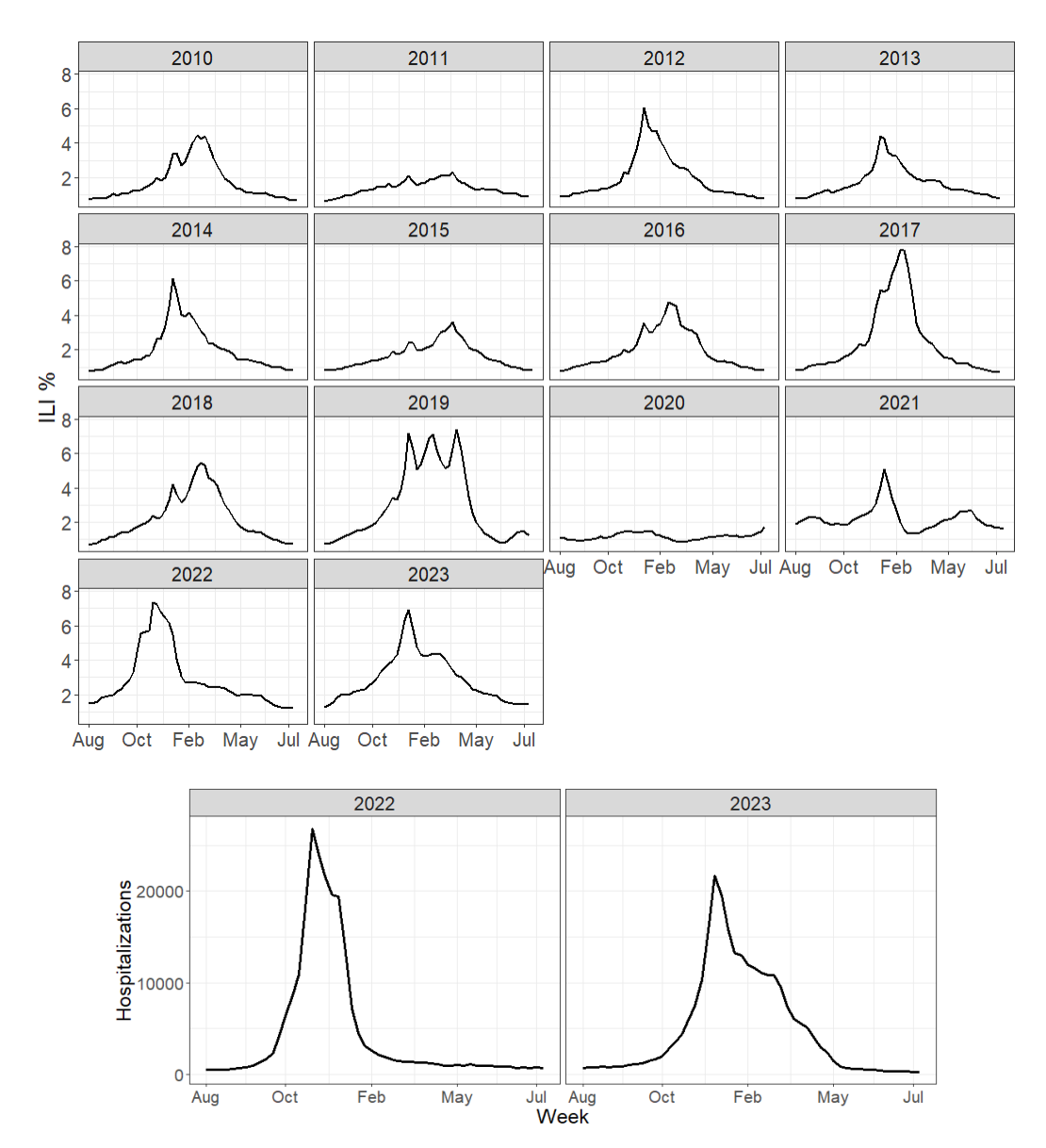


Figure 1: Percentage of outpatient visits with an influenza-like illness (ILI) in the US for seasons 2010 to 2023 (top) and weekly flu confirmed hospitalization counts at the national level for 2022 and 2023 flu seasons (bottom). Week 1 is the first week of August of the year the flu season begins and the last week of the season is the last week of July of the following year.

2024]. Weekly influenza hospitalization data is defined as the number of newly hospitalized patients with a confirmed diagnosis of influenza. From hereon, influenza hospitalizations will be referrred to as hospitalizations.

The bottom of figure 1 shows the weekly national hospitalizations for the 2022 and 2023 flu seasons. These plots show a trend similar to the ILI plots in that during the early weeks of the season hospitalizations are low, but they increase in the fall to a peak and then decrease until the flu outbreak ends. For both the 2022 and 2023 seasons, the hospitalizations peaked during the same week as ILI, and in 2023 that peak occurred during the holiday week 22. Additional plots of ILI data and hospitalization data for all 50 US states are included in the supplementary material [Wadsworth and Niemi, 2024]. These plots show flu outbreak trajectories similar to those in figure 1.

3 ILI and hospitalization forecast modeling

The typical behavior of the ILI data to begin low, rise to a peak, and then fall motivates the use of a nonlinear function which follows a similar trajectory. Compartmental models are standard mathematical models used for modelling disease outbreaks which may capture ILI behavior. One important compartmental model is the susceptible-infectious-recovered (SIR) disease transmission model, which has been used by some to model ILI data [Osthus et al., 2019, Allen, 2017]. The SIR is a mechanistic model used to capture transmission of a particular disease, and since ILI may be influenced by more diseases than influenza, the disease transmission described by the SIR model can only partially contribute to the true ILI data-generating mechanism [Osthus et al., 2019].

Ulloa [Ulloa, 2019] chose to use the asymmetric Gaussian (ASG) function to model ILI data. The ASG is a smooth function which may approximate the same shape as the ILI trajectory. The ASG function has more parameters and is thus slightly more flexible than the SIR model, and thus may be able to roughly capture ILI. However, there may still be systematic behavior which it cannot capture. Thus when using either the SIR or ASG models, an additional component for modeling discrepancy should be included.

In the first part of this section, we present an ILI model similar to the model in Osthus et al. [Osthus et al., 2019]. With some generalization, the model may incorporate any appropriate linear or nonlinear function, though the focus here is on the SIR and ASG functions, defined later in this section. With the aim of forecasting hospitalizations, we also introduce a linear model of hospitalization data with ILI as a predictive covariate. To forecast hospitalizations, ILI data is first forecasted and the forecast is then, as a covariate, plugged into the hospitalization model to produce hospitalization forecasts.

Because we desire probabilistic forecasts, Bayesian modeling is a natural framework for describing forecast uncertainty. Though our main interest is in effeciently producing a probabilistic forecast and not necessarily in estimating model parameters, certain modeling decisions and prior distribution selections proved critical in producing good forecasts. After defining the ILI and hospitalization models, we describe the selection of prior distributions, model fitting, and producing forecasts from the posterior predictive distribution by combining ILI and hospitalization models using a scheme similar to the Bayesian cut [Plummer, 2015].

3.1 ILI Model

The proposed model for ILI for any location is given in (1). Here $ILI_{s,w}$ is the ILI for flu season s and week w=1,2,...,W, where W=52 or W=53, depending on how many Sundays there are in a given season. The ILI is a proportion, so the Beta random variable is a natural selection for modeling. Under the parameterization of the Beta distribution used in (1) the expected value is $\pi_{s,w}$ and the variance is $\pi_{s,w}(1-\pi_{s,w})/(1+\kappa_s)$, making κ_s a scale parameter. The nonlinear function $f_{\theta_s}(w)$ captures the trajectory of the ILI, and γ_w is a discrepancy term shared by all seasons which captures systematic patterns not captured by $f_{\theta_s}(w)$. The additional discrepancy term $v_{s,w}$ captures additional season specific patterns.

$$ILI_{s,w} \stackrel{ind}{\sim} \text{Beta}(\pi_{s,w}\kappa_s, \ \kappa_s(1 - \pi_{s,w}))$$
$$\text{logit}(\pi_{s,w}) = f_{\theta_s}(w) + \gamma_w + \upsilon_{s,w}$$
(1)

In Osthus et al. [Osthus et al., 2019] $f_{\theta_s}(w) = \text{logit}(I_{s,w})$ where $I_{s,w}$ is the infectious compartment of the SIR model from (2) in section 3.2. In Ulloa [Ulloa, 2019], $f_{\theta_s}(w) = ASG_{\theta}(w)$ from (3) in section 3.3. In Ulloa [Ulloa, 2019], modeling is done hierarchically over seasons. Herein we also adopt the hierarchical modeling so as to borrow information contained in the data across all seasons.

Model (1) was fit independently for each location. This decision was made largely due to the limited time given by FluSight to produce forecasts. That is, during the competition, data were typically released on Wednesday afternoons and forecasts were due by the evening of the same day giving only a few hours to produce forecasts. A natural extension of the model would be to allow for states to borrow information from neighboring states.

3.2 Susceptible-Infectious-Recovered (SIR) compartmental model

The SIR compartmental model is a mathematical model used for modeling disease outbreaks and was introduced in 1927 by Kermack and McKendrick [Kermack and McKendrick, 1927]. Since then, compartmental models have become standard in modeling infectious diseases [Allen et al., 2008], and many extensions have been made and studied [Simon, 2020, Allen, 2017, Van den Driessche, 2008, for example]. The SIR mathematical model includes three compartments and assumes that at any time t > 0 every individual in a closed population belongs to exactly one compartment. The

three compartments are susceptible (S), infectious (I), and recovered (R), and their interaction over the course of an outbreak is described by the differential equations in (2).

$$\frac{dS}{dt} = -\beta SI, \quad \frac{dI}{dt} = \beta SI - \delta I, \quad \frac{dR}{dt} = \delta I \tag{2}$$

Here S, I, and R represent the proportion of the population in each compartment such that S+I+R=1 for all t. The trajectory is determined by the disease transmission rate $\beta>0$ and the recovery rate $\delta>0$. Respectively, these may be thought of as the expected proportion of susceptible individuals who will be infected by an infectious individual and the expected rate of recovery to an immune state for a newly infected individual. Whether or not a disease outbreak is classified as an epidemic is determined by the initial susceptible population S_0 , or the susceptible population at time 0, and the parameter $\rho=\delta/\beta$. If $S_0/\rho>1$, the outbreak is considered an epidemic. It is non-epidemic if $S_0/\rho\leq 1$ [Osthus et al., 2019]. Figure 2 shows the trajectory of the three compartments of an SIR model where S_0 and ρ were selected to match an outbreak that is an epidemic. In the case where $S_0 \leq \rho$, the trajectory for the I compartment will be to never increase. The increase to a peak and subsequent decrease in the I compartment of figure 2 illustrate why it is reasonable to use the SIR model to partially capture ILI, although it is unlikely to completely capture the true data generating mechanism. Thus the use of modeling discrepancy.

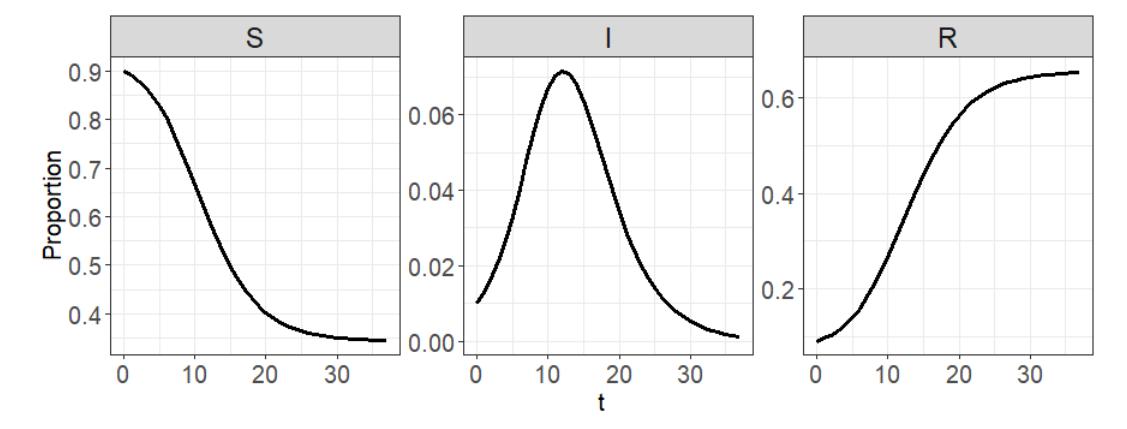


Figure 2: Susceptible-infectious-recovered (SIR) model separated by compartments. The three compartments are the susceptible compartment (left), infectious (center), and recovered (right). In this example, $S_0/\rho > 1$.

3.3 Asymmetric Gaussian (ASG) function

The ASG function is another example of a nonlinear function which can approximate the trajectory of the flu outbreak. The ASG was previously used by Ulloa to model and forecast ILI [Ulloa, 2019]. It has also been used to model vegetation growth and satellite sensor data [Lewis-Beck et al., 2020, Jonsson and Eklundh, 2002, Hird and McDermid, 2009, Beck et al., 2006, Atkinson et al., 2012]. The ASG is a modification of the asymmetric Gaussian distribution [Wallis, 2014] and is characterized by its rise to a peak and fall from that peak, which rise and fall may not occur at the same rate, as shown in figure 3. The ASG function is denoted as $ASG_{\theta}(w)$ where $\theta = (\lambda, \nu, \mu, \sigma_1^2, \sigma_2^2), \nu > 0, \lambda > 0$, $\mu \in (-\infty, \infty), \sigma_1, \sigma_2 > 0$ and $w \in (1, ..., W)$ is week. The function is defined in (3).

$$ASG_{\theta}(w) = \begin{cases} \lambda + (\nu - \lambda) \exp[-(w - \mu)^{2}/2\sigma_{1}^{2}], & w < \mu \\ \lambda + (\nu - \lambda) \exp[-(w - \mu)^{2}/2\sigma_{2}^{2}], & w \ge \mu \end{cases}$$
(3)

In this manuscript, we use a slightly reparameterized version of function (3) shown in (4), where $\eta = \nu - \lambda > 0$. This constraint guarantees that the function has a peak greater than λ .

$$ASG_{\theta}(w) = \begin{cases} \lambda + \eta \exp[-(w - \mu)^{2}/2\sigma_{1}^{2}], & w < \mu \\ \lambda + \eta \exp[-(w - \mu)^{2}/2\sigma_{2}^{2}], & w \ge \mu \end{cases}$$
 (4)

3.4 Model discrepancy

The SIR and ASG functions are useful for capturing the main trend of the ILI data, but as Osthsu et al. [Osthus et al., 2019] point out there may be systematic behavior in the ILI that these or other possible functions may not capture.

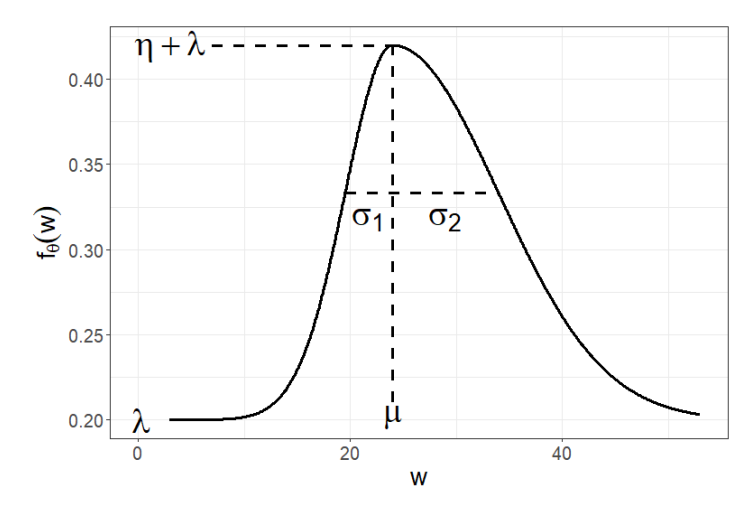


Figure 3: Example plot of asymmetric Gaussian (ASG) function showing the shape of the function in relation to the parameters λ , η , μ , σ_1 , and σ_2

Figures 4 and 5 are used together to illustrate the systematic discrepancy from a fitted function to ILI data. Figure 4 shows the US ILI percentage for all flu seasons from 2010 to 2022 excluding 2020 with a best fit ASG function plotted over the ILI. The fits for each season were made by computing the maximum likelihood estimate (MLE) of a model given the ILI data where we assume the ASG function is the mean parameter of a Beta distributed random variable. Figure 5 shows the discrepancy between the model fit and the data for the same seasons. The grey lines show the difference between the data and the functions from figure 4 for each season, and the black line is the average discrepancy over all seasons. The lines show that the ASG function typically underpredicts week 22 and overpredicts week 23. Perhaps for other weeks, week 30 for example, there tends to be additional systematic behavior not captured by the ASG function.

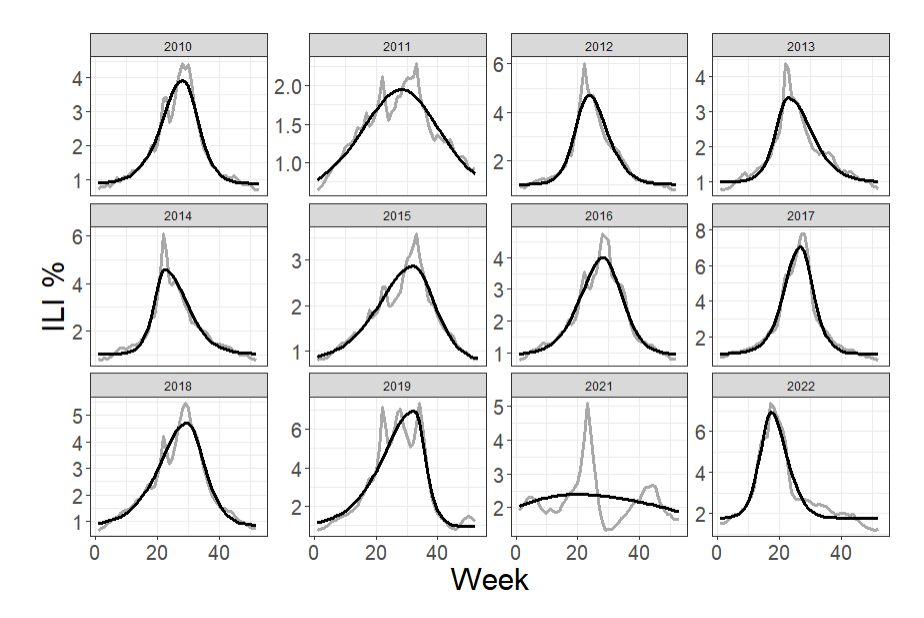


Figure 4: Observed US national influenza-like illness (ILI) percentage for seasons 2010 to 2022 excluding 2020 (grey) overlaid with MLE of an asymmetric Gaussian (ASG) model for the ILI data (black)

Modeling discrepancy has been used in uncertainty analysis of simulators to capture systematic differences between mathematical models and reality [Ma et al., 2022, Brynjarsdóttir and O'Hagan, 2014, Arendt et al., 2012, Kennedy and O'Hagan, 2001]. Modeling discrepancy can lead to overfitting, particularly in forecasting scenarios, and may also lead to identifiability issues. Thus, care must be taken in setting parameter constraints as well as in the selection of prior distributions [Osthus et al., 2019, Brynjarsdóttir and O'Hagan, 2014]. For instance, when setting $f_{\theta_s}(w)$ to be

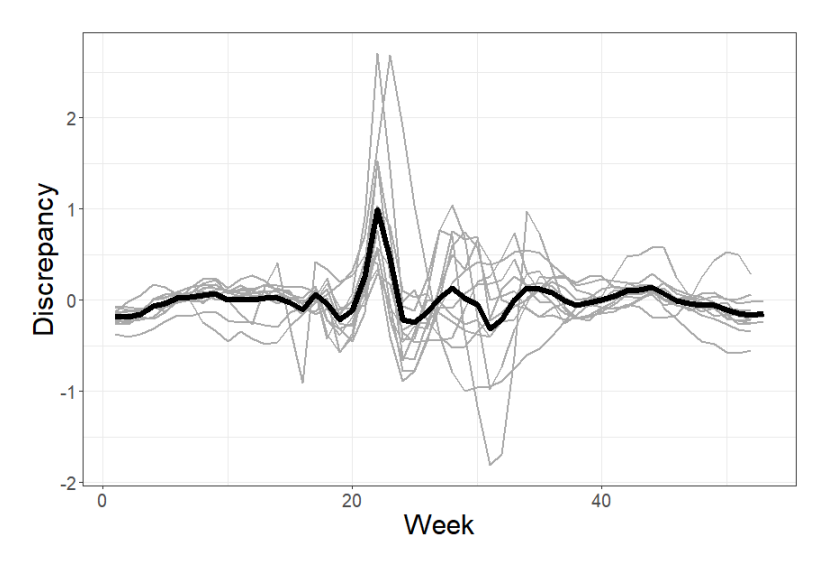


Figure 5: Difference between observed US national influenza-like illness (ILI) and MLE fits for an asymmetric Gaussian (ASG) model for each season 2010 to 2022 excluding 2020 (grey) and the average difference of all seasons (black)

the ASG function in model (1), we found the parameter λ from (4) difficult to estimate precisely because of lack of identifiability. This was resolved by assigning to λ a more informative prior distribution. Modeling of the discrepancy for ILI was done by Osthus et al. during the 2015 and 2016 flu seasons where their model outperformed all others in the CDC flu forecasting challenge [Osthus et al., 2019]. The terms γ_w and $\upsilon_{s,w}$, where s is the season and w is the season week, are included in (1) to capture the per week discrepancy between ILI and the function. Here γ_w is shared across all seasons, whereas $\upsilon_{s,w}$ is specific to season s. To assist in estimating γ_w , $\upsilon_{s,w}$ is only included for the current season being forecast and none of the previous seasons. As in Osthus's model, γ_w and $\upsilon_{s,w}$ are modeled as reverse random walks, as shown in (5).

$$\gamma_{w}|\gamma_{w+1} \stackrel{ind}{\sim} N(\gamma_{w+1}, \sigma_{\gamma}^{2}), \quad \gamma_{W} \sim N(0, \sigma_{\gamma_{W}}^{2})$$

$$\upsilon_{s,w}|\upsilon_{s,w+1} \stackrel{ind}{\sim} N(\upsilon_{s,w+1}, \sigma_{\nu}^{2})$$
(5)

The idea for using the reverse random walk is that there are several previous seasons of ILI data, and assuming the random walk captures systematic behavior, fitting it hierarchically over seasons can assist in predicting future behavior in the current season. Reverse random walks have also been used with success in election forecasting and other flu forecasting models [Osthus and Moran, 2021, Osthus et al., 2019, Linzer, 2013]. The sum to zero constraint $-\gamma_1 = \sum_{w=2}^{W} \gamma_w$ is imposed on (5) to improve identifiability as well as the constraint $v_{s,W} = 0$.

3.5 Hospitalization model

The second component for forecast modeling is based on the relationship between hospitalizations and ILI and is defined in (6). This is an example of an autoregressive model with exogenous variables where the autoregressive lag is one (ARX(1)) [Raftery et al., 2010, Ljung, 1987].

$$H_{s,w} = \alpha_{0s} + \alpha_{1s}(ILI_{s,w} \times P) + \alpha_{2s}(ILI_{s,w} \times P)^2 + \phi H_{s,w-1} + \epsilon_{s,w}$$

$$\epsilon_{s,w} \stackrel{iid}{\sim} D_s(0, \sigma_{\epsilon_s}^2 \times P, \omega_s)$$
(6)

Figure 6 shows US national level data which helps illustrate why this modeling decision was made. The figure shows scatterplots of ILI percentage and hospitalizations on the top row. The bottom row shows scatterplots of the difference between hospitalizations and 1 week lags by ILI percentage. The plots in the right column are of the logarithm of hospitalizations. The lines through the points are drawn by connecting hospitalizations for consecutive weeks during the flu season. These plots show that a linear or quadratic relationship between ILI percentage and hospitalizations does not capture much of the temporal correlation in hospitalizations as shown by the obvious loops drawn in the plot. However, when including a single autoregressive lag of hospitalizations in the model, much of the time correlation is accounted for as shown by the tighter and more frequent crossing of lines in the bottom row. We found that models with more than 1 autoregressive lag showed little or no forecast improvement over 1 lag.

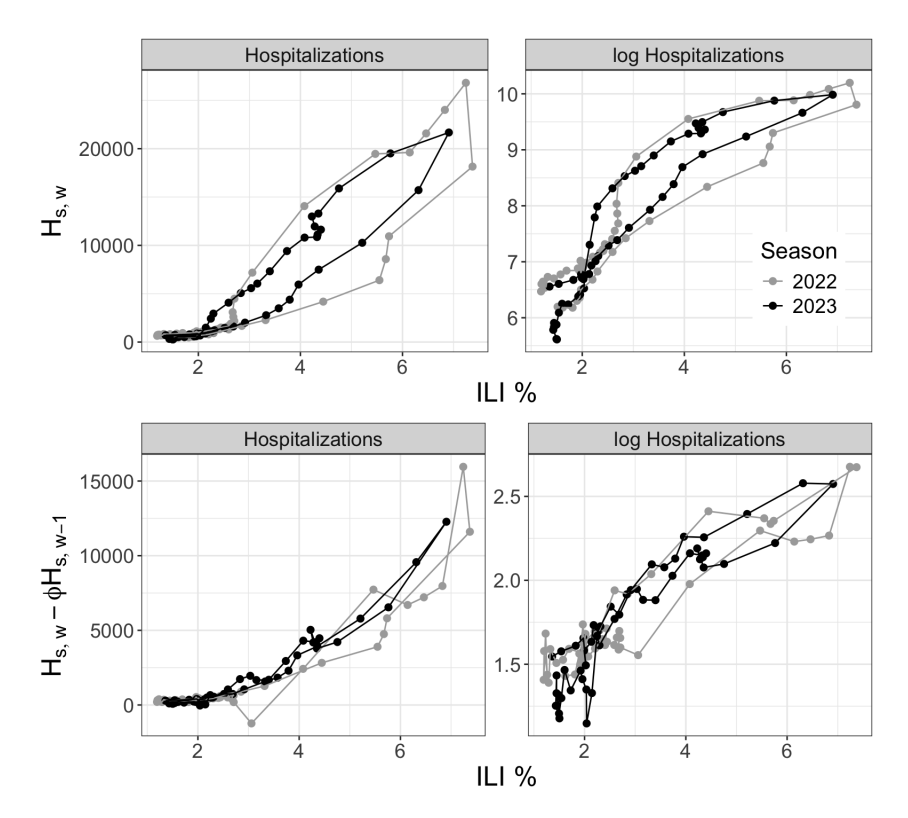


Figure 6: Scatterplots of national hospitalizations (left) or log hospitalizations (right) lag differences by ILI % where the lag is scaled by ϕ . Points are colored by season. For hospitalizations $\phi = 0.6$, and for log hospitalizations $\phi = 0.77$. Lines through the points follow the weekly progression of influenza.

In model (6), $H_{s,w}$ is the number of hospitalizations for week w in season s, $\epsilon_{s,w}$ is an error term distributed according to some distribution D_s with mean parameter 0, scale parameter σ_{ϵ_s} , and the additional parameter ω_s which may be used as degrees of freedom when D_s belongs to the location-scale t (LST) family.

Like the ILI model (1), the hospitalization model was fit independently for each location. For fitting purposes $ILI_{s,w}$ is always multiplied by P which is proportional to the population of the state or territory, in this case the total population divided by 50,000. This is done as a means of scaling so that the prior distribution assigned to $\alpha_s = (\alpha_{0s}, \alpha_{1s}, \alpha_{2s}), \sigma_{\epsilon_s}$, and ω_s might reasonably be the same for all locations.

Like the ILI model, the hospitalization model in (6) is also fit via Bayesian posterior updating. To obtain forecasts for H_{s,w^*+i} , the ILI posterior predictive distribution is used along with the posterior distribution for the parameters in (6). We let D_s belong to the normal family, though in the supplementary materials we present a real forecast analysis where we considered other distribution families including the LST and lognormal families.

3.6 Prior selection

The prior distributions selected for the ILI data model under both the SIR and ASG models largely follow the prior distribution selections in Osthus et al. [Osthus et al., 2019] and Ulloa [Ulloa, 2019] with a few exceptions where selecting different priors improved identifiability, numerical stability, and/or we felt the adjusted prior made more sense for the problem. For model (1), parameters which are common even when using different functions of $f_{\theta_s}(w)$ are κ_s , σ_γ^2 , $\sigma_{\gamma w}^2$, and σ_v . For the SIR function $\theta_s = (S_{0s}, I_{0s}, R_{0s}, \alpha_s, \rho_s)$, and for the ASG function $\theta_s = (\lambda_s, \eta_s, \mu_s, \sigma_{1s}^2, \sigma_{2s}^2)$. For the hospitalization model in (6) the parameter to be estimated is $\Psi = (\alpha_{0s}, \alpha_{1s}, \alpha_{2s}, \phi, \sigma_{\epsilon_s}, \omega_s)$.

The priors assigned were mostly noninformative, though in certain cases the prior distributions were selected for numerical stability as was the case for σ_{γ}^2 and $\sigma_{\gamma_W}^2$. For these two scale parameters only, rather than assigning a half-normal prior to the standard deviation parameters, as recommended by Gelman [Gelman, 2006], the priors were assigned to the variance parameters. Univariate parameters were assigned either a normal distribution prior if the support was on \mathbb{R} , a half-normal prior if the support is nonnegative, or a truncated-normal prior to match a more specific support.

Under the ASG model, θ_s was modeled hierarchically over seasons so that for each season the transformed parameter $T(\theta_s) \sim N(\theta, \Sigma)$ and priors distributions are assigned to θ and Σ where $T(\theta_s) = (\lambda_s, \log(\eta_s), \mu_s, \log(\sigma_{1s}^2), \log(\sigma_{2s}^2))$.

Additional prior constraints were made to improve parameter identifiability. Just as was done in Osthus et al. [Osthus et al., 2019], we set the initial value of the susceptible population compartment of the SIR model was set to $S_0 = 0.9$. The parameters I_{0s} , β_s , and ρ_s were assigned informative priors. In a previous version of this manuscript, when fitting an ASG model with discrepancy components, rather than estimating all parameters through posterior updating, identifiability was encouraged by setting the parameter λ_s from (4) to be equal to its MLE. In this updated manuscript, however, we use empirical Bayes and center the first component of the hierarchal prior θ to be the mean of MLEs for λ_s across all seasons and set the variance parameter so the prior was tight around the mean. This led to improved mixing of posterior draws and better forecasts. The specific prior distributions assigned to each parameter are listed in the supplementary materials.

3.7 Hospitalization Forecasts Using the Bayesian Cut

Rather than combining the ILI model in equation (1) with the hospitalization model in equation (6) and fitting a single posterior distribution, both models were fit separately and 1 to 4 week ahead ILI forecasts from model (1) were combined with the posterior predictive distribution of model (6) to obtain 1 to 4 week ahead hospitalization forecasts. In this scheme, the posterior distribution of model (1) parameters was not directly influenced by the hospitalization data and the posterior distribution of model (6) parameters was not directly influenced by model (1) parameters. Hence there was limited feedback between the two components, but propagation of uncertainty in ILI forecasts was still permitted in the estimating of hospitalization forecasts.

This two-component modeling is remeniscent of the Bayesian cut described in Plummer [2015] and Nott et al. [2023]. Cutting a model into two component models or "modules" may be justfied for several reasons including to reduce time to fit the model, avoiding mixing issues of posterior sampling distributions, improving predictive performance or to prevent model misspecification in one model to influence the other [Nott et al., 2023, Jacob et al., 2020, 2017, Plummer, 2015].

The decision to cut the forecast model into two component models was made for several reasons. When fitting the fully Bayesian joint model, the time to fit a single model using Markov chain Monte Carlo (MCMC) sampling and obtain forecasts was sometimes many hours whereas fitting the two models separately took a fraction of the time. When assessing convergence of model parameters, it was rare that posterior sampling chains for the joint model showed convergence even after 55,000 iterations, whereas the component model fits gave no signs which raised concern for convergence. And most importantly, the forecasts from the component models generally outperformed those of the joint model in terms of minimizing proper scoring rules.

Model (1) was fit via Bayesian posterior updating. Future ILI forecasts were obtained via the posterior predictive distribution where for week w, the predictive distribution was obtained by integrating over the parameters π_s , κ_s , σ_γ^2 , and $\sigma_{\gamma w}^2$ as in (7) where $p(\pi_s, \kappa_s, \sigma_\gamma^2, \sigma_{\gamma w}^2 | \mathbf{ILI})$ is the density function of the posterior distribution for the model parameters. If the current week was w then the desired forecasts were for weeks w + i where i is a positive integer. Here $\widehat{ILI}_{s,w+i}$ represents the predicted or forecasted ILI at i weeks in the future.

$$p(\widetilde{ILI}_{s,w+i}|\mathbf{ILI}) = \int \int \int \int p(\widetilde{ILI}_{s,w+i}|\boldsymbol{\pi}_s, \kappa_s, \sigma_{\gamma}^2, \sigma_{\gamma_w}^2) p(\boldsymbol{\pi}_s, \kappa_s, \sigma_{\gamma}^2, \sigma_{\gamma_w}^2|\mathbf{ILI}) d\boldsymbol{\pi}_s d\kappa_s d\sigma_{\gamma}^2 d\sigma_{\gamma_w}^2$$
(7)

Hospitalization forecasts $H_{s,w+i}$ at week w+i were then obtained by combining the posterior predictive distribution of model (6) with (7) and integrating over $\widetilde{ILI}_{s,w+i}$ as in (8). Here, α represents all regression and variance parameters in model (6).

$$p(\tilde{H}_{s,w+i}|\mathbf{ILI},\mathbf{H},\alpha) = \int p(\tilde{H}_{s,w+i}|\mathbf{H},\mathbf{ILI},\widetilde{ILI}_{s,w+i},\alpha)p(\widetilde{ILI}_{s,w+i}|\mathbf{ILI})d\widetilde{ILI}_{s,w+i}$$
(8)

3.8 Parameter estimation and posterior predictive sampling

The models were fit via MCMC sampling using the cmdstanr package which was developed and is maintained by the Stan Development Team [Stan Development Team, 2024] [Gabry et al., 2024]. Stan implements Hamiltonian Monte Carlo (HMC) sampling with the No-U-turn sampler [Hoffman et al., 2014]. The cmdstanr package provides several diagnostic statistics for assessing the sampler. Plots of prior and posterior distributions for select parameters from ILI and hospitalization models are included in the supplementary material [Wadsworth and Niemi, 2024].

Model fit was assessed for four ILI models and for the hospitalization model. The ILI models included the SIR and ASG models and models with and without discrepancy modeling. When discrepancy is included, the models are denoted as SIRD and ASGD. These models were fit using US national data from 2010 to 2023 flu seasons, where data from the 2020 season was excluded because of the unique behavior during that season. Sampling was done with four chains where from each chain 60,000 posterior draws were sampled, and the first 10,000 draws were discarded as a burn-in. The \hat{R} statistic [Vehtari et al., 2021] and the effective sample size (ESS) [Gelman et al., 2013] were calculated for each parameter, and for all models fit, the largest \hat{R} was below the recommend threshold of 1.05, and the smallest ESS was over 500.

To obtain forecast distributions of hospitalizations, draws from the posterior predictive distribution from the ILI model were used in conjunction with the posterior distribution of the hospitalizations model. When fitting model (7), MCMC samples of $\widetilde{ILI}_{s,w:(w+4)}$ were saved. Model (6) was fit and MCMC samples for the marginal distributions for the model parameters were saved. To obtain forecast distributions for $H_{s,w+i}$ where $i \in \{1,2,3,4\}$, the following steps were repeated K times where K is an integer for the number of desired samples. We set K = 50,000.

```
Step 1: Sample \widetilde{ILI}_{s,w:(w+4)}^*
Step 2: Sample \alpha_{0s}^*, \alpha_{1s}^*, \alpha_{2s}^*, \phi^*, \sigma_{\epsilon_s}^*, \omega_s^* from respective marginal posterior distributions
Step 3: Sample H_{s,w+i}^* from D(\omega_s^*, \mu_{s,w+i}^*, \sigma_{\epsilon_s}^2), where
```

 $\mu_{s,w+i}^* = \alpha_{0s}^* + \alpha_{1s}^* (ILI_{s,w+i}^* \times P) + \alpha_{2s}^* (ILI_{s,w+i}^* \times P)^2 + \phi^* H_{s,w+i-1}^*$ Step 4: Repeat step 3 for $i \in \{1,2,3,4\}$ to obtain $H_{s,(w+1):(w+4)}^*$

Step 5: Repeat steps 1-4 K times

The sample $\{H_{s,w+i}^*\}^K$ was then used as the probabilistic forecast for hospitalizations at week w+i. Occasionally $\{H_{s,w+i}^*\}^K$ included a small number of negative values, which do not make sense when the distribution is meant to forecast hospitalizations, a nonnegative number. We attempted to alleviate this problem by modeling log-hospitalizations or by assuming hospitalizations followed a distribution truncated at 0, but these models led to poorer forecasts and issues drawing from the posterior distribution. For the forecast competition analysis in section 5, all negative values of $\{H_{\mathfrak{c},w\pm i}^*\}^K$ were set to 0 to reflect realistic values of hospitalizations and comply with the FluSight forecasting rules.

Simulation Study

In this section, we present a simulation study conducted for comparing ILI models and further assessing the hospitalization forecast model. US ILI data is used, and hospitalization data is simulated. A leave-one-season-out (LOSO) approach was combined with a Monte Carlo simulation approach. For each replication, we simulated log-hospitalizations for all weeks during seasons 2010, ..., 2022, excluding 2020, using the existing ILI data as a predictive covariate. Each season was in turn "left-out" and treated as if it was the most recent season for which forecasts are desired. Fitting and forecasting was then done for weeks 14, 20, 26, 32, and 38 of the left out season, giving two weeks that tend to occur as flu cases increase, two as cases decrease, and one that occurs when the cases may be increasing or decreasing. Week 20 is a week leading up to the holiday week 22 where ILI typically has a local peak. We were particularly interested in how important modeling discrepancy is for forecasting at week 20.

Besides the 4 ILI models, we also included forecasts for a naive baseline (BASE) model and an autoregressive integrated moving average (ARIMA) model. The BASE model is a simple random walk with drift model, and the ARIMA model is fit by selecting the best possible model give the data according to a fitting criterion. Both the BASE and ARIMA ILI models were fit using the forecast package in R Hyndman and Khandakar [2008].

For the simulation of hospitalizations, the parameters $\alpha_s = (\alpha_{0s}, \alpha_{1s}, \alpha_{2s})$ and $\sigma_{\epsilon_s}^2$ from the hospitalization model in (6) were considered the same across all seasons so that all $\alpha_s = \alpha$. Note that this is not a model assumption we make but only a simplyfying assumption for simulating the data. The values for α , σ_{ϵ}^2 , and ϕ were estimated by fitting model (6) using ILI and hospitalization data from the 2022 season. For fitting, the hospitalization data was first log-transformed. We took $\alpha_{\phi} = (\alpha, \phi)$ and assigned the noninformative prior $p(\alpha_{\phi}, \sigma_{\epsilon}^2) \propto 1/\sigma_{\epsilon}^2$. The marginal posterior distribution $\alpha_{\phi}|\sigma_{\epsilon}^2, H_{22}$ was then the established posterior multivariate normal distribution and $\sigma_{\epsilon}^2|H_{22}$ the inverse- χ^2 posterior distribution [Gelman et al., 2013]. The posterior means of those parameters were used as the values from which log-hospitalizations were simulated. The number of replicates in the simulation was 500.

Model comparison was done by calculating a proper scoring rule for each forecast. Proper scoring rules are the current standard for comparing performance between probabilistic forecasts and selecting the best forecasts according to the notion of maximizing sharpness subject to (auto-)calibration [Gneiting et al., 2007, Tsyplakov, 2013]. Proper scoring rules are commonly used in forecast comparison, and they are designed such that a forecaster is incentivized to be honest in the reporting of their forecasts [Gneiting and Raftery, 2007, Gneiting and Katzfuss, 2014]. The proper scoring rule primarily used in the FluSight competition and the COVID-19 Forecast Hub, and which is used in this simulation study, is the negatively oriented (smaller is better) weighted interval score (WIS) [Mathis et al., 2024, Bracher et al., 2021]. The WIS is used for scoring quantile or interval forecasts, or forecasts made up of predictive intervals of several nominal levels [Gneiting and Raftery, 2007, Gneiting and Katzfuss, 2014, Bracher et al., 2021]. The WIS defined in (9) where Q is a forecast represented by all included quantiles, B is the number of intervals, y^* is the observed value targeted by the forecast, $w_0 = 1/2$ and $w_b = \alpha_b/2$ are weights for each interval, and α_b is the nominal level of the b^{th} interval where $b \in \{1, ..., B\}$. IS_α is the interval score (IS), a proper scoring rule for a single interval, defined in (10). Here $1\{\cdot\}$ is the indicator function.

$$WIS_{0,B}(Q, y^*) = \frac{1}{B+1/2} \times (w_0 \times |y^* - median| + \sum_{b=1}^{B} \{w_k \times IS_{\alpha_b}(Q, y^*)\})$$
(9)

$$IS_{\alpha}(l,r;y^*) = (r-l) + \frac{2}{\alpha}(l-y^*)\mathbb{1}\{y^* < l\} + \frac{2}{\alpha}(y^*-r)\mathbb{1}\{y^* > r\}$$
(10)

The forecasts used in this section and in the subsequent section follow the FluSight convention of being quantiles corresponding to the 23 given probabilities

(0.010, 0.025, 0.050, 0.100, 0.150, ..., 0.950, 0.975, 0.990) making each forecast a set of 11 predictive intervals and a predictive median. Figure 7 gives three plots showing results of the study. Plot a) shows WIS scores averaged over each left out season and each of the 500 simulation replicates. The ASGD forecasts on average clearly outperformed the other models considered in almost every week. The ASGD does especially well at week 20 which contains forecasts of the holiday week 22. This demonstrates the particular importance of modeling discrepancy at and around that week. The SIRD outperforms the SIR model, again showing the importance of modeling discrepancy, but it is still outperformed by the ASG and even for a few weeks by the BASE and ARIMA models. Plot b) shows boxplots of all forecast scores by model and separated by horizon forecasts of 1 to 4 weeks ahead. Here also the ASGD performs the best with the other variations of the nonlinear models not always outperforming the BASE or ARIMA models. To assess calibration, plot c) shows the empirical coverage of each model for 11 predictive intervals from 10% to 98% nominal levels. Each model is undercalibrated, but the ASGD model is the closest to being well calibrated, especially at the hightest nominal levels. Table 1 shows summaries of the mean WIS and coverage for 50% and 95% predictive intervals.

Table 1: Summary values of forecast performance in simulation study for ASGD, ASG, SIRD, SIR, BASE, and ARIMA models. WIS, 50% and 95% predictive interval coverage averaged over all seasons and 500 simulation replicates.

Model	WIS	50%Coverage	95% Coverage
ASGD	0.02	0.42	0.91
ASG	0.03	0.33	0.71
ARIMA	0.03	0.35	0.68
BASE	0.03	0.33	0.65
SIRD	0.03	0.33	0.78
SIR	0.05	0.20	0.51

The results of this simulation study demonstrate the effectiveness of using the assymetric Gaussian function along with modeling discrepancy for modeling ILI and making flu hospitalization forecasts in the US. The following section shows similar effectiveness of coupling an effective ILI flu model with a hospitalization model to forecast hospitalizations during the 2023 flu season.

5 Analysis of forecasts for 2023 flu season

In this section we apply the forecast models to make forecasts for the 2023 flu season weekly hospitalizations and compare the results with those of forecasts submitted to FluSight. The scoring of the forecasts is in the context of the FluSight competition where each competing forecast was submitted as a set of 23 quantiles corresponding to given probabilities. Forecasts of 1, 2, 3, and 4-week ahead hospitalization counts were requested, and forecasts were made at the state and national levels. The first week of forecasting took place during the week of October 7, 2023, and the final week was the week of May 4, 2024 making 30 total weeks of forecasts. The same format was used during the 2021 and 2022 seasons and for the COVID-19 Forecast Hub [Mathis et al., 2024, Bracher et al., 2021]. Primary scores for evaluating each forecast were the WIS and the log-weighted intveral score (LWIS). The LWIS is defined the same as

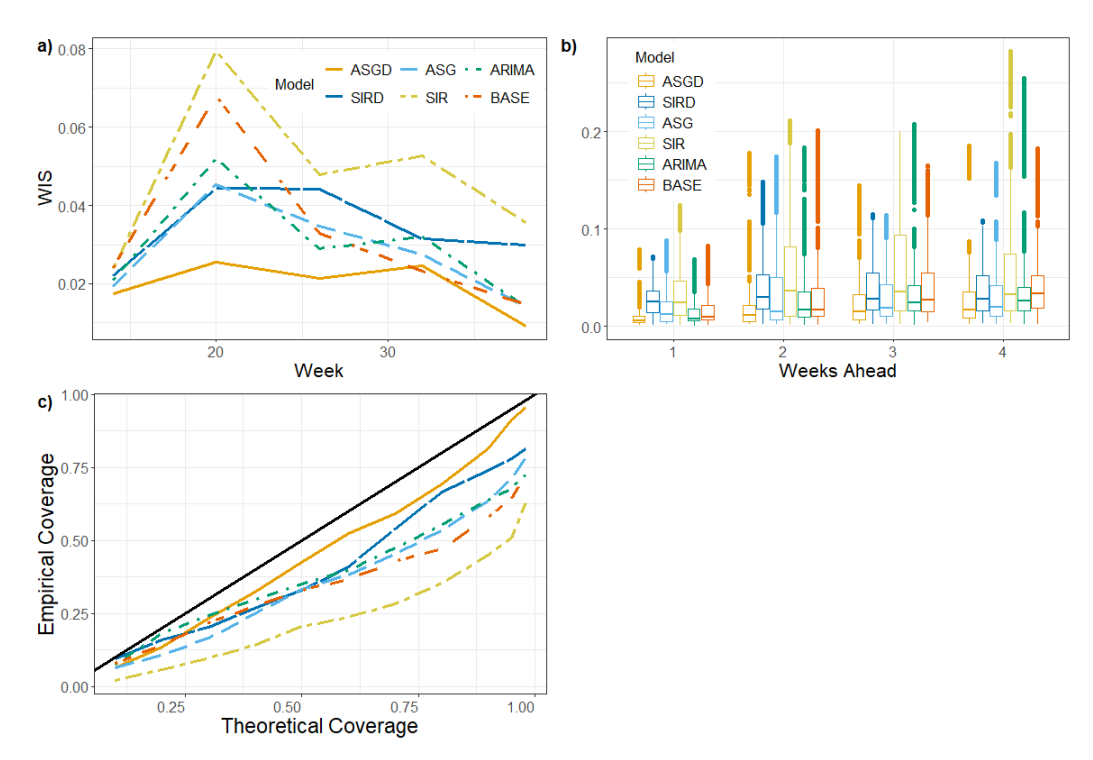


Figure 7: Results of forecasts for simulated hospitalizations for ASGD, ASG, SIRD, SIR, BASE, and ARIMA models. Plot a), WIS averaged over all left out seasons and 500 simulation replicated for each of weeks 14, 20, 26, 32, and 38, coloured by model. Plot b), boxplots of all WIS scores separated by forecast horizon of 1 to 4 weeks ahead. Plot c), empirical calibration of each forecast model as the overall forecast coverage of predictive intervals for the 11 nominal levels 10%, 20%, ..., 90%, 95%, 98%.

the WIS but where the log of the observation as well as the log forecast quantiles are taken prior to calculating the score. We primarily use the LWIS in this section, though we including results for the WIS in the supplementary materials.

Figure 8 shows hospitalization forecasts at four different weeks during the season for ASGD, ASG, SIRD, and SIR ILI models where hospitalizations are modeled according to model (6) where ILI is a quadratic predictor of hospitalizations, and hospitalizations are assumed to be normally distributed. Of these forecasts, the ASGD appears to do the best job at capturing the trajectory of hospitalizations as well as most frequently making the sharpest predictions, particularly later in the season.

For the remainder of this section, focus will be made on forecasts made by coupling the ASGD and SIRD models with the normal hospitalization model where ILI is a quadratic predictor. These forecast schemes are denoted as ASGD_NORM2 and SIRD_NOMR2. In the supplementary materials, we include analysis of 2023 hospitalization forecasts for several other forecast models including ASG and SIR ILI models coupled with other variations of the hospitalization model where the ASGD_NORM2 showed the best results and the SIRD_NORM2 performed nearly as well as the ASGD_NORM2.

The FluSight models which are used for comparison are the 20 non-ensemble models submitted to FluSight during the 2023 season. The submitted forecasts may be found at Github [2024]. Among the models was the FluSight baseline. The baseline forecast had as a median the most recently observed hospitalization count, and the forecast uncertainty was based on differences between previous hospitalizations. The baseline forecast model was similar to the baseline forecast model used in previous flu forecasting seasons and in the COVID-19 hub [Mathis et al., 2024, Cramer et al., 2022].

Figure 9 shows forecast results for the 2023 flu hospitalization forecasts for all 22 models being compared but with results for the ASGD_NORM2, SIRD_NORM2, and FluSight baseline models highlighted. For each week of the 2023 season, the LWIS averaged over location and horizon for each model is shown in a). Boxplots of LWIS for 1, 2, 3, and 4-week ahead horizons for the ASGD_NORM2, SIRD_NORM2, and baseline models are shown in b). And overall empirical coverage of the 11 predictive intervals for all models is shown in c) with ASGD_NORM2, SIRD_NORM2 and the baseline model highlighted. These plots show that over the season the ASGD_NORM2 model tended to outperform most others in terms of LWIS, and in general is superior to the baseline model. The coverage plot shows that the

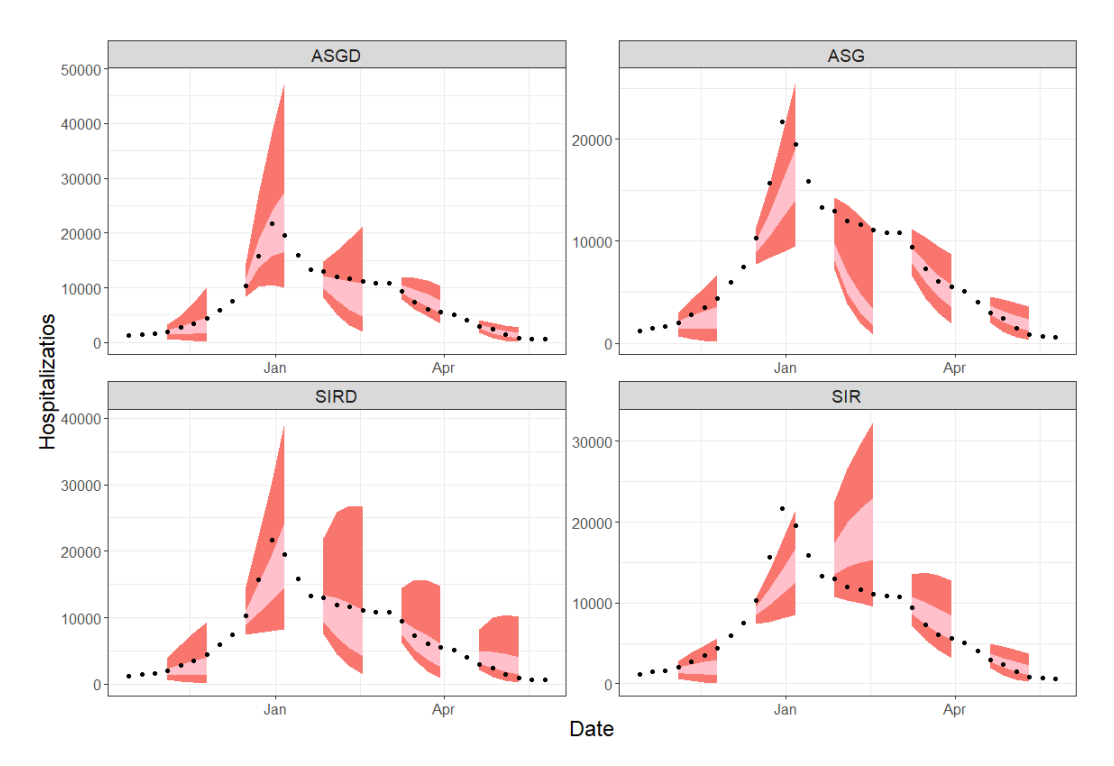


Figure 8: Forecasts 1-4 weeks ahead for US hospitalizations during the 2023 season for weeks 14, 20, 26, and 32. Forecasts are separated by ILI model, and the hospitalization models are all normally distributed and ILI is a quadratic predictor.

ASGD_NORM2 model is well calibrated at most levels, with slight overcoverage at the lower levels up to about 80%, and has better coverage than all other models. Similar results for the WIS are shown in the supplementary materials.

During the FluSight competition, most participating teams would occasionally miss a forecast submission for some week, location, or horizon. This makes a simple average of scores an imperfect measure for comparison, as forecasts of certain targets included for one model may be excluded by another model. Thus in figure 10 the ASGD_NORM2 model is compared with all other models individually using LWIS scores averaged over only the forecasts shared by the two models. Each tile represents the ratio of average ASGD_NORM2 LWIS to that of one FluSight model by location or by week. We call this the relative LWIS (RLWIS). A value smaller than 1 indicates the ASGD_NORM2 model outperforms the competing model. A value higher than 1 indicateds the ASGD_NORM2 is outperformed. A grey tile indicates the competing model had no forecasts matching the specified target. Similar plots showing WIS scores are found in the supplementary materials. The ASGD_NORM2 outperforms most other competing models more often than not, but there are some weeks or locations where forecasting was poorer. For example, the plot shows the ASGD_NORM2 performed poorly in Montana relative to most other models.

Table 2 gives summary results for mean and median WIS and LWIS scores, predictive coverage, and relative RWIS and RLWIS scores for each model. Along with the plots in this section, it shows that over the course of the 2023 season, the ASGD_NORM2 outperformed every other model except the UGA_flucast-INFLAenza. The SIRD_NORM2 is also one of the top performing forecast models.

6 Conclusion

In this manuscript we introduce a statistical modeling framework which allows for the incorporation of several nonlinear ILI forecast modeling methods. Specifically, we built upon Osthus et al. [Osthus et al., 2019] and introduced a framework for modeling ILI which includes the use of an arbitrary function for modeling the main trajectory of ILI along with modeling the discrepancy and specifically incorporate the smooth ASG function. We model flu hospitalizations by incorporating the ILI forecast model into a model forecasting hospitalizations where hospitalization predictions are a linear or quadratic function of ILI. Utilizing the ILI data which has been available for many more years than flu hospitalization, greatly improves one's ability to forecast hospitalizations, and the borrowing information from all

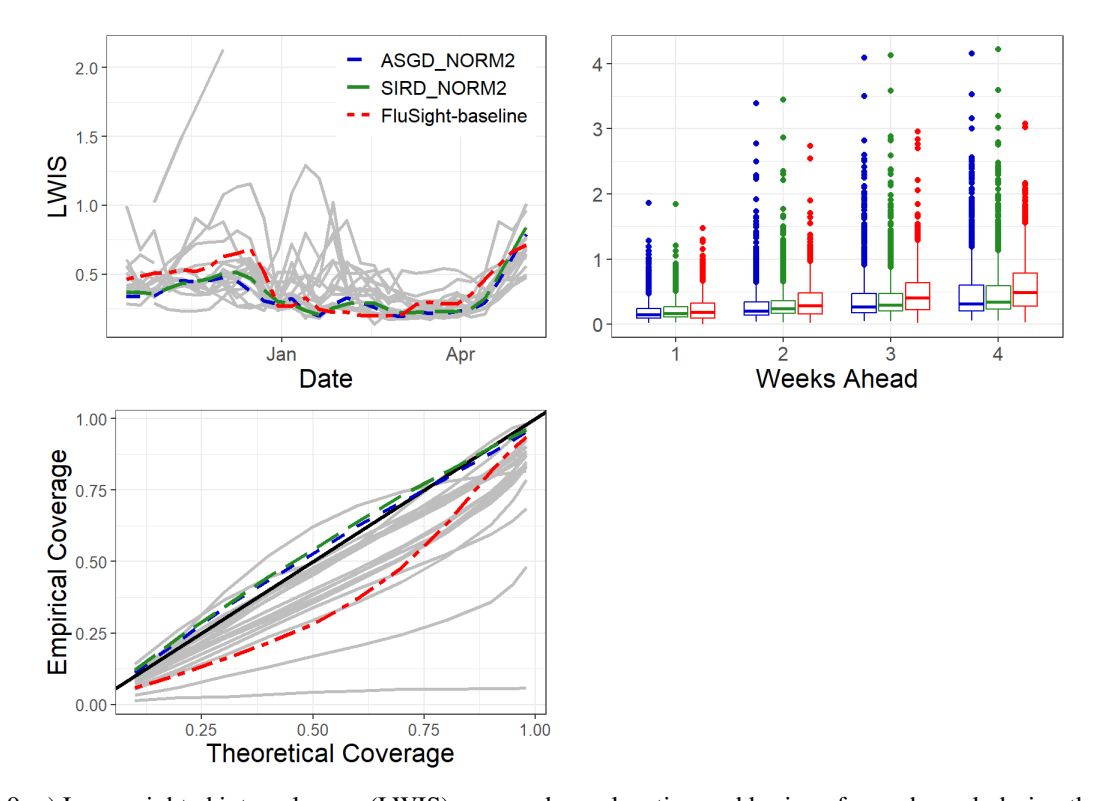


Figure 9: a) Log-weighted interval score (LWIS) averaged over location and horizon for each week during the season for the 21 models being compared. Each grey line represents one model, but the ASGD_NORM2 (blue), SIRD_NORM2 (green), and FluSight-baseline (red) are colored to stand out. b) Boxplots of all LWIS scores for 1, 2, 3, and 4-week ahead horizons for the ASGD_NORM2 (blue) and FluSight-baseline (red) models. c) Plot of empirical coverage against theoretical coverage for 11 predictive intervals from the 10% nominal level to the 98%. The black line x = y shows where optimal coverage would fall. Each grey line represents one model, but the ASGD_NORM2 (blue), SIRD_NORM2 and FluSight-baseline (red) are colored to stand out.

previous seasons through hierarhetical modeling is able to further exploit the ILI data. Including model discrepancy was an important piece of successful forecasting, but it required making thoughtful model constraints and selection of prior distributions.

The simulation study in section 4 suggests the ASGD function in ILI modeling outperforms the SIRD model and out of the box forecast methods according to the WIS scoring rule, and in the analysis of 2023 FluSight forecasts the ASGD_NORM2 modeling scheme outperformed all but one of the competing forecasts when looking at the whole season. Though the ASGD_NORM2 did very well across the whole season, there were a small number of weeks or locations where performance was not as good. It should not be assumed that ASGD_NORM2 forecasts would perform as well in every season given that each flu season will come with its own challenges which the modeling scheme may or may not address.

The models in this manuscript were such that the data in each location were modeled as independent from all other locations. It is reasonable to assume that a disease outbreak in one state will share characteristics with the outbreak in neighboring states, and indeed the behavior of ILI and hospitalizations is more closely related for neighboring states as shown in data plots in the supplementary materials. Notably, the one 2023 FluSight forecast model which outperformed the ASGD_NORM2, the UGA_flucast-INFLAenza, was listed as being a spatial model. And in past seasons, some of the top performing forecast models also explicitly modeled spatial relationships [Osthus and Moran, 2021]. Likewise, the forecasts to which ours was compared were all non-ensemble forecasts which were all outperformed by the ensemble forecasts in FluSight. Futher extensions of the models herein could include explicit modeling of spatial relationships between states and inclusion in an ensemble of other forecast models.

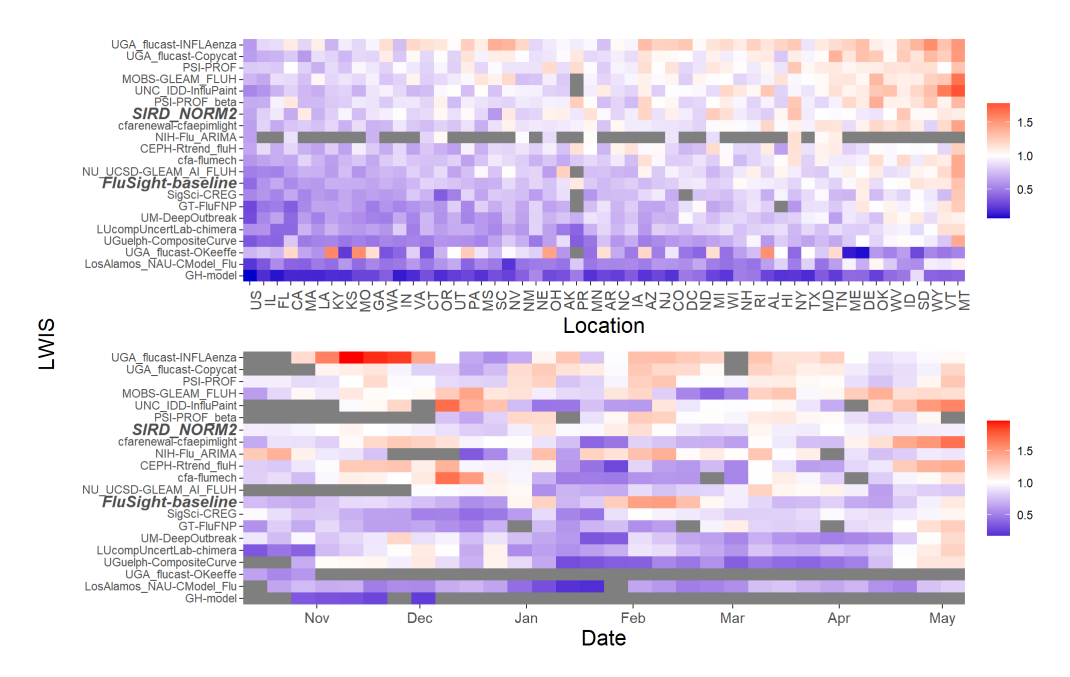


Figure 10: Ratio of average log-weighted interval score (LWIS) for ASGD_NORM2 to that of each competing FluSight model. Scores are averaged over all targets within indicated location (top) or week (bottom) and only include forecasts shared by both models. Lower scores (blue) indicate superior performance by the ASGD_NORM2 model and higher scores (red) indicate superior performance by competing model.

7 References

Linda JS Allen. A primer on stochastic epidemic models: Formulation, numerical simulation, and analysis. *Infectious Disease Modelling*, 2(2):128–142, 2017.

Linda JS Allen, Fred Brauer, Pauline Van den Driessche, and Jianhong Wu. *Mathematical Epidemiology*, volume 1945. Springer, 2008.

Paul D Arendt, Daniel W Apley, Wei Chen, David Lamb, and David Gorsich. Improving identifiability in model calibration using multiple responses. *Journal of Mechanical Design*, 134(10):100909, 2012.

Peter M Atkinson, C Jeganathan, Jadu Dash, and Clement Atzberger. Inter-comparison of four models for smoothing satellite sensor time-series data to estimate vegetation phenology. *Remote Sensing of Environment*, 123:400–417, 2012.

Pieter SA Beck, Clement Atzberger, Kjell Arild Høgda, Bernt Johansen, and Andrew K Skidmore. Improved monitoring of vegetation dynamics at very high latitudes: A new method using MODIS NDVI. *Remote Sensing of Environment*, 100(3):321–334, 2006.

Matthew Biggerstaff, David Alper, Mark Dredze, Spencer Fox, Isaac Chun-Hai Fung, Kyle S Hickmann, Bryan Lewis, Roni Rosenfeld, Jeffrey Shaman, Ming-Hsiang Tsou, et al. Results from the Centers for Disease Control and Prevention's predict the 2013–2014 Influenza Season Challenge. *BMC Infectious Diseases*, 16(1):1–10, 2016.

Johannes Bracher, Evan L Ray, Tilmann Gneiting, and Nicholas G Reich. Evaluating epidemic forecasts in an interval format. *PLOS Computational Biology*, 17(2):e1010592, 2021.

Jennỳ Brynjarsdóttir and Anthony O'Hagan. Learning about physical parameters: The importance of model discrepancy. *Inverse Problems*, 30(11):114007, 2014.

CDC. Centers for Disease Control and Prevention FluView portal. https://gis.cdc.gov/grasp/fluview/fluportaldashboard.html, 2024a. Accessed: 2024-10-22.

CDC. Centers for Disease Control and Prevention FluSight: About flu forecasting. https://www.cdc.gov/flu-forecasting/about/index.html?CDC_AAref_Val=https://www.cdc.gov/flu/weekly/flusight/how-flu-forecasting.htm, 2024b. Accessed: 2024-10-22.

CDC. Centers for Disease Control and Prevention FluView, U.S. influenza surveillance: Purpose and methods. https://www.cdc.gov/fluview/overview/?CDC_AAref_Val=https://www.cdc.gov/flu/weekly/overview.htm, 2024c. Accessed: 2024-10-22.

Table 2: Overall summary scores for each of the 20 non-ensemble FluSight models and the ASGD_NORM2 model. Summaries include mean weighted interval and log-weighted interval scores (MWIS/MLWIS), median weighted interval and log-weighted interval scores (MedWIS/MedLWIS), mean squared error difference between predictive model empirical and theoretical coverage (MSEC) see figure 9 c)), percentage of forecasts for all targets during the 2023 season (% Forcs), and relative weighted interval and log-weighted interval scores (RWIS/RLWIS).

	MWIS	MLWIS	MedWIS	MedLWIS	MSEC	% Forcs	RWIS	RLWIS
ASGD_NORM2	62	0.34	14	0.23	0.001	100	1	1
PSI-PROF	63	0.35	15	0.23	0.003	100	0.90	0.97
SIRD_NORM2	67	0.36	16	0.26	0.001	100	0.93	0.95
CEPH-Rtrend_fluH	69	0.39	13	0.28	0.004	100	0.81	0.86
FluSight-baseline	85	0.41	16	0.32	0.023	100	0.63	0.82
UM-DeepOutbreak	83	0.46	21	0.39	0.010	99	0.64	0.72
cfarenewal-cfaepimlight	76	0.37	15	0.26	0.001	99	0.72	0.92
MOBS-GLEAM_FLUH	66	0.35	15	0.22	0.021	98	0.87	0.95
LosAlamos_NAU-CModel_Flu	242	0.64	24	0.42	0.153	93	0.21	0.53
UGuelph-CompositeCurve	132	0.52	25	0.41	0.018	93	0.43	0.62
LUcompUncertLab-chimera	84	0.43	17	0.33	0.004	92	0.67	0.71
UGA_flucast-INFLAenza	74	0.32	15	0.20	0.003	90	0.77	1.07
cfa-flumech	101	0.41	17	0.27	0.019	89	0.58	0.85
UGA_flucast-Copycat	76	0.35	16	0.21	0.012	87	0.81	0.98
GT-FluFNP	105	0.48	18	0.38	0.046	86	0.45	0.73
UNC_IDD-InfluPaint	107	0.35	16	0.24	0.043	78	0.58	0.95
NU_UCSD-GLEAM_AI_FLUH	98	0.39	22	0.24	0.014	74	0.68	0.83
SigSci-CREG	59	0.49	12	0.31	0.018	71	0.62	0.74
PSI-PROF_beta	77	0.32	18	0.20	0.004	67	0.87	0.93
NIH-Flu_ARIMA	230	0.34	28	0.23	0.001	20	0.57	0.88
GH-model	161	1.52	28	1.47	0.373	17	0.18	0.27
UGA_flucast-OKeeffe	27	0.59	8	0.43	0.003	10	0.60	0.58

Estee Y Cramer, Yuxin Huang, Yijin Wang, Evan L Ray, Matthew Cornell, Johannes Bracher, Andrea Brennen, Alvaro J Castro Rivadeneira, Aaron Gerding, Katie House, Dasuni Jayawardena, Abdul H Kanji, Ayush Khandelwal, Khoa Le, Jarad Niemi, Ariane Stark, Apurv Shah, Nutcha Wattanachit, Martha W Zorn, Nicholas G Reich, and US COVID-19 Forecast Hub Consortium. The United States COVID-19 forecast hub dataset. *Scientific Data*, 9(1):462, 2022. URL https://doi.org/10.1038/s41597-022-01517-w.

Anne Ewing, Elizabeth C Lee, Cécile Viboud, and Shweta Bansal. Contact, travel, and transmission: the impact of winter holidays on influenza dynamics in the United States. *The Journal of Infectious Diseases*, 215(5):732–739, 2017.

Jonah Gabry, Rok Češnovar, and Andrew Johnson. cmdstanr: R Interface to 'CmdStan', 2024. R package version 0.7.1, https://discourse.mc-stan.org.

Roberto C Garza, Ricardo Basurto-Dávila, Ismael R Ortega-Sanchez, Luis Oreste Carlino, Martin I Meltzer, Rachel Albalak, Karina Balbuena, Pablo Orellano, Marc-Alain Widdowson, and Francisco Averhoff. Effect of winter school breaks on influenza-like illness, Argentina, 2005–2008. *Emerging Infectious Diseases*, 19(6):938, 2013.

Andrew Gelman. Prior distributions for variance parameters in hierarchical models. *Bayesian Analysis*, 1(3):515–533, 2006.

Andrew Gelman, John B Carlin, Hal S Stern, David B Dunson, Aki Vehtari, and Donald B Rubin. *Bayesian Data Analysis, Third Edition*. Chapman and Hall/CRC, 2013.

Github. FluSight-forecast-hub. https://github.com/cdcepi/FluSight-forecast-hub, 2024. Accessed: 2024-10-22.

Tilmann Gneiting and Matthias Katzfuss. Probabilistic forecasting. *Annual Review of Statistics and Its Application*, 1: 125–151, 2014.

Tilmann Gneiting and Adrian E Raftery. Strictly proper scoring rules, prediction, and estimation. *Journal of the American Statistical Association*, 102(477):359–378, 2007.

Tilmann Gneiting, Fadoua Balabdaoui, and Adrian E Raftery. Probabilistic forecasts, calibration and sharpness. *Journal of the Royal Statistical Society Series B: Statistical Methodology*, 69(2):243–268, 2007.

HealthData.gov. COVID-19 reported patient impact and hospital capacity by state (raw). https://healthdata.gov/dataset/COVID-19-Reported-Patient-Impact-and-Hospital-Capa/6xf2-c3ie/about_data, 2024. Accessed: 2024-10-22.

- Jennifer N Hird and Gregory J McDermid. Noise reduction of NDVI time series: An empirical comparison of selected techniques. *Remote Sensing of Environment*, 113(1):248–258, 2009.
- Matthew D Hoffman, Andrew Gelman, et al. The No-U-Turn sampler: adaptively setting path lengths in Hamiltonian Monte Carlo. *Journal of Machine Learning Research*, 15(1):1593–1623, 2014.
- Rob J Hyndman and Yeasmin Khandakar. Automatic time series forecasting: the forecast package for R. *Journal of Statistical Software*, 27(3):1–22, 2008. doi: 10.18637/jss.v027.i03.
- Pierre E Jacob, Lawrence M Murray, Chris C Holmes, and Christian P Robert. Better together? statistical learning in models made of modules. *arXiv* preprint arXiv:1708.08719, 2017.
- Pierre E Jacob, John O'leary, and Yves F Atchadé. Unbiased markov chain monte carlo methods with couplings. *Journal of the Royal Statistical Society Series B: Statistical Methodology*, 82(3):543–600, 2020.
- Per Jonsson and Lars Eklundh. Seasonality extraction by function fitting to time-series of satellite sensor data. *IEEE ransactions on Geoscience and Remote Sensing*, 40(8):1824–1832, 2002.
- Susan L Joslyn and Jared E LeClerc. Uncertainty forecasts improve weather-related decisions and attenuate the effects of forecast error. *Journal of Experimental Psychology: Applied*, 18(1):126, 2012.
- Marc C Kennedy and Anthony O'Hagan. Bayesian calibration of computer models. *Journal of the Royal Statistical Society: Series B Statistical Methodology*, 63(3):425–464, 2001.
- William Ogilvy Kermack and Anderson G McKendrick. A contribution to the mathematical theory of epidemics. Proceedings of the Royal Society of London. Series A, Containing papers of a mathematical and physical character, 115(772):700–721, 1927.
- Colin Lewis-Beck, Victoria A Walker, Jarad Niemi, Petruţa Caragea, and Brian K Hornbuckle. Extracting agronomic information from SMOS vegetation optical depth in the US Corn Belt using a nonlinear hierarchical model. *Remote Sensing*, 12(5):827, 2020.
- Drew A Linzer. Dynamic Bayesian forecasting of presidential elections in the states. *Journal of the American Statistical Association*, 108(501):124–134, 2013.
- L Ljung. System Identification: Theory for the User. Prentice-Hall, Englewood Cliffs, NJ, 1987.
- Chelsea S Lutz, Mimi P Huynh, Monica Schroeder, Sophia Anyatonwu, F Scott Dahlgren, Gregory Danyluk, Danielle Fernandez, Sharon K Greene, Nodar Kipshidze, Leann Liu, et al. Applying infectious disease forecasting to public health: a path forward using influenza forecasting examples. *BMC Public Health*, 19(1):1–12, 2019.
- Pulong Ma, Georgios Karagiannis, Bledar A Konomi, Taylor G Asher, Gabriel R Toro, and Andrew T Cox. Multifidelity computer model emulation with high-dimensional output: An application to storm surge. *Journal of the Royal Statistical Society Series C: Applied Statistics*, 71(4):861–883, 2022.
- Sarabeth M Mathis, Alexander E Webber, Tomás M León, Erin L Murray, Monica Sun, Lauren A White, Logan C Brooks, Alden Green, Addison J Hu, Roni Rosenfeld, et al. Evaluation of FluSight influenza forecasting in the 2021–22 and 2022–23 seasons with a new target laboratory-confirmed influenza hospitalizations. *Nature Communications*, 15(1):6289, 2024.
- Thomas McAndrew and Nicholas G Reich. Adaptively stacking ensembles for influenza forecasting. *Statistics in Medicine*, 40(30):6931–6952, 2021.
- Craig J McGowan, Matthew Biggerstaff, Michael Johansson, Karyn M Apfeldorf, Michael Ben-Nun, Logan Brooks, Matteo Convertino, Madhav Erraguntla, David C Farrow, John Freeze, et al. Collaborative efforts to forecast seasonal influenza in the United States, 2015–2016. *Scientific Reports*, 9(1):683, 2019.
- Noelle-Angelique M Molinari, Ismael R Ortega-Sanchez, Mark L Messonnier, William W Thompson, Pascale M Wortley, Eric Weintraub, and Carolyn B Bridges. The annual impact of seasonal influenza in the US: measuring disease burden and costs. *Vaccine*, 25(27):5086–5096, 2007.
- David J Nott, Christopher Drovandi, and David T Frazier. Bayesian inference for misspecified generative models. *Annual Review of Statistics and Its Application*, 11, 2023.
- Dave Osthus and Kelly R Moran. Multiscale influenza forecasting. Nature Communications, 12(1):2991, 2021.
- Dave Osthus, James Gattiker, Reid Priedhorsky, and Sara Y Del Valle. Dynamic Bayesian influenza forecasting in the United States with hierarchical discrepancy (with discussion). *Bayesian Analysis*, 14(1):261–312, 2019.
- Martyn Plummer. Cuts in bayesian graphical models. Statistics and Computing, 25:37–43, 2015.
- Adrian E Raftery, Miroslav Kárnỳ, and Pavel Ettler. Online prediction under model uncertainty via dynamic model averaging: Application to a cold rolling mill. *Technometrics*, 52(1):52–66, 2010.

- Maria H Ramos, Schalk J Van Andel, and Florian Pappenberger. Do probabilistic forecasts lead to better decisions? *Hydrology and Earth System Sciences*, 17(6):2219–2232, 2013.
- Evan L Ray, Nutcha Wattanachit, Jarad Niemi, Abdul Hannan Kanji, Katie House, Estee Y Cramer, Johannes Bracher, Andrew Zheng, Teresa K Yamana, Xinyue Xiong, et al. Ensemble forecasts of coronavirus disease 2019 (COVID-19) in the US. *medRxiv*, pages 2020–08, 2020.
- Bob Rudis. cdcfluview: Retrieve Flu Season Data from the United States Centers for Disease Control and Prevention ('CDC') 'FluView' Portal, 2021. URL https://CRAN.R-project.org/package=cdcfluview. R package version 0.9.4.
- Cory M Simon. The SIR dynamic model of infectious disease transmission and its analogy with chemical kinetics. *PeerJ Physical Chemistry*, 2:e14, 2020.
- Stan Development Team. Stan modeling language users guide and reference manual, 2.34. https://mc-stan.org, 2024. Accessed: 2024-10-22.
- Alexander Tsyplakov. Evaluation of probabilistic forecasts: proper scoring rules and moments. *Available at SSRN* 2236605, 2013.
- James Turtle, Pete Riley, Michal Ben-Nun, and Steven Riley. Accurate influenza forecasts using type-specific incidence data for small geographic units. *PLOS Computational Biology*, 17(7):e1009230, 2021.
- Nehemias Ulloa. *Bayesian hierarchical modeling for disease outbreaks*. PhD thesis, Iowa State University Department of Statistics, 2019.
- P Van den Driessche. Deterministic compartmental models: extensions of basic models. In *Mathematical Epidemiology*, pages 147–157. Springer, 2008.
- Aki Vehtari, Andrew Gelman, Daniel Simpson, Bob Carpenter, and Paul-Christian Bürkner. Rank-normalization, folding, and localization: An improved \hat{R} for assessing convergence of MCMC (with discussion). *Bayesian Analysis*, 16(2):667–718, 2021.
- Spencer Wadsworth and Jarad Niemi. Supplement to forecasting influenza hospitalizations using a bayesian hierarchical nonlinear model with discrepancy, 2024.
- Kenneth F Wallis. The two-piece normal, binormal, or double Gaussian distribution: its origin and rediscoveries. *Statistical Science*, pages 106–112, 2014.
- WHO. World Health Organization website influenza (seasonal) fact sheet. https://www.who.int/news-room/fact-sheets/detail/influenza-(seasonal), 2024. Accessed: 2024-10-22.
- Robert L Winkler. Probabilistic prediction: Some experimental results. *Journal of the American Statistical Association*, 66(336):675–685, 1971.
- Teresa K Yamana, Sasikiran Kandula, and Jeffrey Shaman. Superensemble forecasts of Dengue outbreaks. *Journal of The Royal Society Interface*, 13(123):20160410, 2016.